International Journal of Engine Research
http://jer.sagepub.com/

Study of the mixture formation processes inside a modern direct-injection gasoline engine

P Koch, M G Löffler, M Wensing and A Leipertz

International Journal of Engine Research 2010 11: 455
DOI: 10.1243/14680874JER606

The online version of this article can be found at:
http://jer.sagepub.com/content/11/6/455

Published by:
SAGE
http://www.sagepublications.com

On behalf of:
Institution of Mechanical Engineers
Institution of Mechanical Engineers

Study of the mixture formation processes inside a modern direct-injection gasoline engine

P Koch[1,2], **M G Löffler**[1,2], **M Wensing**[1,2], and **A Leipertz**[1,2]*
[1]Lehrstuhl für Technische Thermodynamik, Universität Erlangen-Nürnberg, Erlangen, Germany
[2]Erlangen Graduate School in Advanced Optical Technologies, Friedrich-Alexander-Universität Erlangen-Nürnberg, Erlangen, Germany

The manuscript was accepted after revision for publication on 13 September 2010.

DOI: 10.1243/14680874JER606

Abstract: The combustion process inside a direct injection spark ignition engine with charge stratification is a very complex process with a large number of variables existing for the definition of the engine characterization map. In this work, two different tracer-based laser-induced fluorescence techniques were applied to analyse the charge motion during the mixing process. For two different operation points with and without a complex in-cylinder flowfield, the two-line excitation LIF technique was applied for temperature and residual gas fraction imaging, and the FARLIF technique for fuel/air ratio imaging. It was found that the mixing of air and residual gas was very fast, and hence no inhomogeneities were found at ignition time. For the mixture preparation process, the swirl makes it difficult to position the fuel vapour cloud near the spark plug at ignition. As a solution to overcome this, a double-injection strategy was applied. With careful parameter choice, depending on the second injection mass and timing, the desired charge situation could be achieved.

Keywords: DISI, optical engine, tracer-LIF, residual gas, mixture formation, fuel/air ratio

1 INTRODUCTION

The combustion process inside a direct injection engine is very complex. For its design and engineering, a detailed knowledge of the involved subprocesses and their interaction within the functioning chain forming the complete engine process is needed. In modern gasoline combustion concepts the application of direct injection in combination with stratification and the reduction of throttling losses is one of the most promising strategies. Owing to the small timescales of mixture preparation and the inhomogeneities of the cylinder charge, a large number of variables exist for the definition of the engine characterization map. Varying injection timings with the use of multipoint injections, air-, wall-, or jet-guided mixture formation, and exhaust gas recirculation are only some examples for variation possibilities [**1**]. Owing to the numerous different reactions that take place and show a great dependence on the ambient conditions, the chemical reaction of the fuel is already a highly sophisticated process. Additionally, in engine combustion, temperature and pressure change rapidly, and the reaction field is superposed by a complex flowfield and, in some cases, by a mixing field. In particular, the ignitability of the fuel/air mixture has to be guaranteed at all operating points. As a useful tool for the design and engineering, a direct view into the cylinder during mixture formation and combustion is becoming more and more important. Non-invasive, laser-based measurement techniques are commonly used and often provide the only possibility to obtain the desired information [**2**]. In the present work a direct injection spark ignition gasoline engine with charge stratification was examined under part-load operation using two different forms of tracer-based laser-induced fluorescence.

**Corresponding author: Lehrstuhl für Technische Thermodynamik, Universität Erlangen-Nürnberg, Am Weichselgarten 8, Erlangen 91058, Germany.*
email: Alfred.Leipertz@ltt.uni-erlangen.de; sek@ltt.uni-erlangen.de

2 THEORETICAL BACKGROUND

To gain insight into the mixture formation and the combustion process, appropriate optical diagnostic tools have been applied to the modified optical engine. Here, two well-known fluorescence tracer substances, acetone and triethylamine (TEA), were applied to analyse the mixture formation process using two different measurement techniques. Both techniques are based on laser-induced fluorescence (LIF) and allow a two-dimensional visualization and determination of the desired quantities, fuel/air ratio, temperature, and residual gas distribution. Both techniques deliver time-resolved image series by use of pulsed lasers, and in both cases the non-fluorescent component isooctane was used as a substitute for gasoline fuel. In commercial gasoline, each component shows individual fluorescence properties, and therefore a quantitative determination of the desired data is not possible. With isooctane it is possible to realize defined chemical and spectroscopic fuel properties at low absorption values.

The first technique applied is the two-line excitation LIF technique with the tracer acetone (see, for example, Thurber *et al.* [**3**]). With this technique, the temperature field and the fraction of the intake air can be quantified, which is, as a first approximation, inverse to the concentration of the residual gas fraction. The second measurement technique is the fuel/air ratio laser-induced fluorescence technique (FARLIF) introduced by Reboux and Puechberty [**4**], with TEA as tracer. Using FARLIF, the fuel/air ratio can be quantified in the vapour phase and the distribution of the liquid phase can be imaged qualitatively. Both techniques take advantage of the frequency red shift, which makes it possible to separate with optical filters the signal from the scattered and reflected light of the excitation wavelength, which is usually strong inside engines. Even though both techniques are based on laser-induced fluorescence, the main influences on the signal strength differ significantly.

2.1 Two-line excitation LIF

For the visualization of the residual gas fields, acetone is a well-suited tracer owing to its high vapour pressure and its broad absorption spectrum in the ultraviolet region. Dominant non-collision deactivation rates make the fluorescence at atmospheric pressure relatively insensitive to bath gas composition and quenching by oxygen [**5**]. Additionally, acetone is stable against decomposition up to temperatures of 1000 K under short residence times.

In the linear regime, i.e. when the fluorescence intensity depends linearly on the excitation energy, the fluorescence signal S is proportional to the optical efficiency η, the pulse energy E, the tracer number density ρ_{acetone}, the absorption cross-section σ_{acetone}, and the fluorescence quantum yield ϕ_{acetone}

$$S \propto \eta \cdot E \cdot \rho_{\text{acetone}} \cdot \sigma_{\text{acetone}}(\lambda, T) \cdot \phi_{\text{acetone}}(\lambda, p, T, \chi_i) \quad (1)$$

where the absorption cross-section σ_{acetone} is a function of wavelength λ and temperature T, and the fluorescence quantum yield ϕ_{acetone} is a function of wavelength, temperature, pressure p, and gas composition χ_i of the colliding molecules. Collisions with molecules such as nitrogen lead to vibrational relaxation and thereby increase the yield ϕ_{TEA}. Collisions with oxygen can lead to intersystem crossing to a triplet state or deactivation, which reduces the fluorescence signal strength [**6**]. As S is also a function of the excitation wavelength λ, it is possible to eliminate tracer density inhomogeneities in the plane of observation by applying the two-line excitation method. Thus, two subsequent LIF images with different excitation wavelengths are acquired quasi-simultaneously and divided by each other, so the tracer number density cancels out. In the present work, excitation wavelengths of 248 and 308 nm of two excimer lasers were used

$$\frac{S_{308}}{S_{248}} = \frac{\eta_{308} \cdot E_{308} \cdot \sigma_{308}(T) \cdot \phi_{308}(T, p, \chi_i)}{\eta_{248} \cdot E_{248} \cdot \sigma_{248}(T) \cdot \phi_{248}(T, p, \chi_i)} \quad (2)$$

To eliminate the optical efficiency, a reference is taken with known pressure, temperature, and gas composition and identical optical parameters. With normalization to this reference and the known laser pulse energy, the signal ratio is only a function of temperature, pressure, and bath gas composition

$$S_{\text{R,norm}} = \frac{S_{308,\text{norm}}}{S_{248,\text{norm}}} = f(T, p, \chi_i) \quad (3)$$

$$S_{308,\text{norm}} = f(T, p, \chi_i) \quad (4)$$

The pressure can be conveniently taken from a conventional in-cylinder pressure transducer, and only two unknown variables are then left. In an IC engine, the bath gas composition can be considered to be a binary system of intake air and exhaust gas, while often the small fraction of fuel vapour can be neglected. Therefore, the tracer density is directly

proportional to the fraction of fresh intake air if the tracer is added in the intake manifold

$$\rho_{\text{tracer}} \propto \chi_{\text{tracered air}} = 1 - \chi_{\text{EGR}} \tag{5}$$

Under this assumption, the temperature and tracer density can be determined iteratively from equations (3) and (4).

The signal intensities have to be calibrated for the desired temperature and pressure range. Because of the weak influence of the bath gas on the LIF signal, the used calibration data cover only pure air and a synthetic 50:50 air–exhaust gas mixture. In the image processing code, the influence of bath gas composition was weighted linearly according to the actual amount of EGR. These calibration data, which were used here for calculation of the results, can be found in Löffler *et al.* [**7**], where also the image processing is described in more detail.

2.2 FARLIF

In a large part of the operating range of DISI engines, FARLIF can be used as a relatively robust method for determination of the fuel/air ratio. If the tracer TEA is added to the fuel, the signal strength is proportional to the fuel/air ratio and independent of the pressure above a certain minimum oxygen partial pressure. For TEA, this limit is given by a total pressure of 3 bar in air [**8**]. Hence, only the dependence of the signal on temperature has to be calibrated. Detailed information on LIF can be found, for example, in Daily [**9**], a detailed description of FARLIF is given by Schulz and Sick [**6**], and the limitations are discussed, for example, by Koban *et al.* [**10**]. Here, a short description is given following Koban *et al.* [**11**].

In the linear excitation regime, the fluorescence signal is proportional to the optical efficiency η, the pulse energy E, the tracer number density ρ_{TEA}, the absorption cross-section σ_{TEA}, and the fluorescence quantum yield ϕ_{TEA}

$$S \propto \eta \cdot E \cdot \rho_{\text{TEA}} \cdot \sigma_{\text{TEA}}(\lambda, T) \cdot \phi_{\text{TEA}}(\lambda, p, T, \chi_i) \tag{6}$$

The absorption cross-section depends on excitation wavelength and temperature, and the fluorescence quantum yield depends on excitation wavelength, pressure, temperature, and the bath gas composition of the colliding molecules. In contrast to acetone, collisions of TEA with oxygen can lead to electronic de-excitation, which is referred to as quenching and reduces the signal strength strongly. The effect of quenching on fluorescence can be described by the rates of the deactivation processes

$$\phi_{\text{TEA}} = \frac{k_{\text{fl}}}{k_{\text{total}} + \tilde{k}^{\text{O}_2}_{\text{quench}} \rho_{\text{O}_2}} \tag{7}$$

where k_{fl} is the fluorescence rate (s^{-1}), k_{total} is the total sum of all intramolecular de-excitation rates, and $\tilde{k}^{\text{O}_2}_{\text{quench}}$ is the bimolecular quenching rate coefficient, which depends on the number density of oxygen ρ_{O_2} and is therefore usually labelled with a tilde. The impact of oxygen quenching is typically measured relative to the total intramolecular de-excitation rate. This ratio is called the Stern–Volmer factor, k_{SV}

$$k^{\text{O}_2}_{\text{SV}} = \frac{\tilde{k}^{\text{O}_2}_{\text{quench}}}{k_{\text{total}}} \tag{8}$$

This factor can be deduced as the slope from a Stern–Volmer plot. There, the inverse signal, normalized to the signal without the quencher oxygen, is plotted against the oxygen concentration

$$\frac{S}{S_0} - 1 = \frac{k_{\text{fl}}}{k_{\text{total}}} \frac{k_{\text{total}} + \tilde{k}^{\text{O}_2}_{\text{quench}} \rho_{\text{O}_2}}{k_{\text{fl}}} = k_{\text{SV}} \rho_{\text{O}_2} \tag{9}$$

The fluorescence quantum yield can now be written in terms of rates and the Stern–Volmer factor

$$S \propto \rho_{\text{TEA}} \sigma_{\text{TEA}} \cdot \frac{k_{\text{fl}}/k_{\text{total}}}{1 + k_{\text{SV}} \rho_{\text{O}_2}} \tag{10}$$

When the quenching of oxygen is the dominant de-excitation process, the product of Stern–Volmer factor and number density of oxygen is all dominant in the denominator. Then, and for constant temperature, the fluorescence signal strength from TEA added to the fuel is directly proportional to the fuel/air ratio

$$S \propto \frac{\rho_{\text{TEA}}}{\rho_{\text{O}_2}} \propto \Phi \quad \text{for } k_{\text{SV}} \rho_{\text{O}_2} \gg 1 \tag{11}$$

The signal strength is independent of the number density of tracer and of the bath gas composition, i.e., if the cylinder is filled with a mixture of residual gas, air, and fuel with tracer, the fuel/air ratio is visible independently of the fraction of residual gas. The conditions of proportionality are given typically with high cylinder pressures where the number density of oxygen is also high. It must be mentioned that the total pressure above which equation (11) is valid increases with higher temperatures and larger fractions of

residual gas. The calibration of the temperature influence to the signal strength can be done directly in the engine and is described below in section 3.2.

3 EXPERIMENTAL SET-UP

3.1 Engine

The measurements have been performed in a single-cylinder optical engine based on a series-production direct injection engine with four valves per cylinder. The specifications of the engine and of the experimental set-up are summarized in Table 1.

The optical access was provided by a window in the bottom of the piston and a glass ring replacing the upper half of the cylinder liner (see Fig. 1). A nose-like extension on the upper side of the ring (the hump on the right-hand side of the glass ring in Fig. 1) enables access to the spark plug area. It is possible to illuminate or detect the signal through the glass ring or, depending on the requirements, through the piston. To keep this glass ring clean, contact to the piston rings has to be avoided. This elongates the free gap of the piston ring, which results in an increased compression space and a reduced compression ratio. A mirror is placed inside the elongated, slotted piston, and, depending on the optical set-up, it was either used for the irradiation of the laser light sheet or for the detection of signals. Figure 1 shows schematic drawings of the engine, with its optical accesses, and the experimental set-ups using a horizontal (HLLS) or a vertical laser light sheet (VLLS). For fluorescence excitation, two different excimer lasers have been

Table 1 Engine and experimental set-up data

Number of cylinders	1
Number of valves	4
Stroke/bore	85 mm/77 mm
Spark plug location	Central
Injector location	Lateral
Injector	Seven-hole high-pressure injection system
Optical access	Transparent cylinder liner with access to spark plug area, sloped window in extended piston

	FARLIF	Acetone-LIF
Fuel	Isooctane	
Tracer	TEA (added to fuel)	Acetone (added to intake air)
Excitation wavelength	248 nm	248 and 308 nm
Detection range	~ 275–300 nm	> 355 nm
Camera	Double-shutter ICCD	
Lens	UV 100 mm f/2.0	

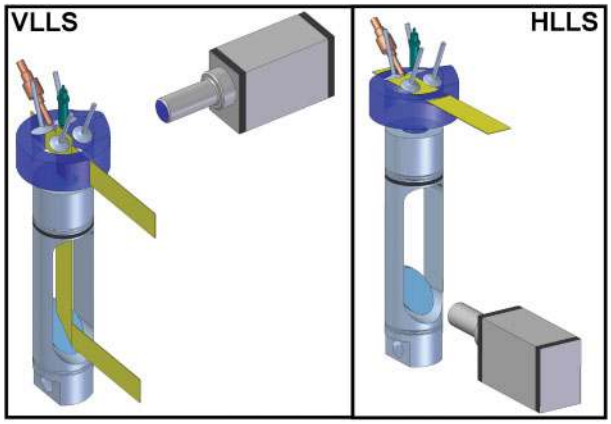

Fig. 1 Experimental set-up for the mixture formation investigation

used. To enlarge the illuminated area of the vertical light sheet, the laser is directed from the bottom and from the side simultaneously in the cylinder for the FARLIF experiments. The field of view and the position of the horizontal light sheet are shown in Fig. 2. The horizontal light sheet has been positioned as close as possible to the spark plug near the upper edge of the glass ring.

By using a conditioning system, the temperature of the engine's oil and water cycle was kept constant

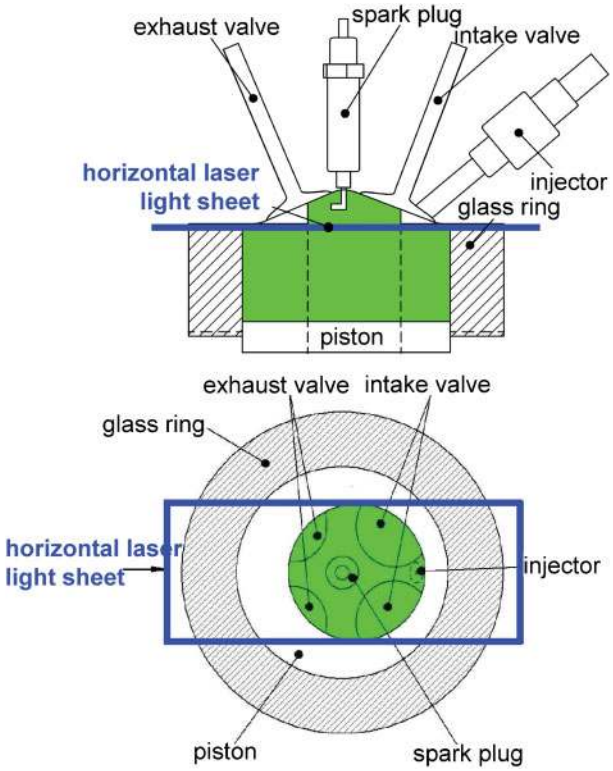

Fig. 2 Fields of view for the FARLIF measurements. The green areas indicate the image planes (VLLS: top; HLLS: bottom)

at 353 K for all measurements. The engine was mounted onto a 180 kW engine test bench which controlled the constant speed at 1500 r/min. In motored operation, no fuel was injected, whereas the ignition was still operating. In continuous fired operation mode, the engine was run with both fuel injection and spark ignition.

3.2 FARLIF

To obtain an in-cylinder LIF calibration image, it was necessary to supply the engine with a premixed homogeneous mixture of well-known fuel/air ratio. For this requirement, a premixing pipe was fitted to the intake manifold of the transparent engine (Fig. 3). With this set-up it was possible to run the engine either at ideally premixed or direct injection conditions. For the calibration, the fuel was injected into the mixing pipe with a high-pressure swirl injector controlled by an external trigger unit. Thus, it was possible to adjust the fuel/air ratio using a λ-sensor while the engine was running. In this case, a λ-value of 1.0 was adjusted. To avoid condensation of fuel inside the premixing pipe, the pipe walls were heated up to 373 K. To intensify the evaporation and to homogenize the mixture, several turbulence parts were inserted into the pipe. The fuel supply of the premixing injector was realized by a constant-pressure diaphragm system operated up to 10 MPa.

3.2.1 *Acquisition procedure*

Using the electrical motor to run the transparent engine, it was possible to switch between motored, premixed, or direct injection operations. Before the start of the measurements, all parameters were adjusted. For each crank angle measurement, at first 16 images at motored operation (background correction) and then 16 images at premixed operation (homogeneous before, $\lambda = 1.0$ calibration) were conducted. After this, 16 images at direct injection (measurement) and finally 16 images at premixed operation (homogeneous after, $\lambda = 1.0$ calibration) were taken. For fluorescence excitation, a KrF-excimer laser was applied. Example images of these measurements using the horizontal laser light sheet can be seen in Fig. 4. This procedure was carried out for all crank angle scans.

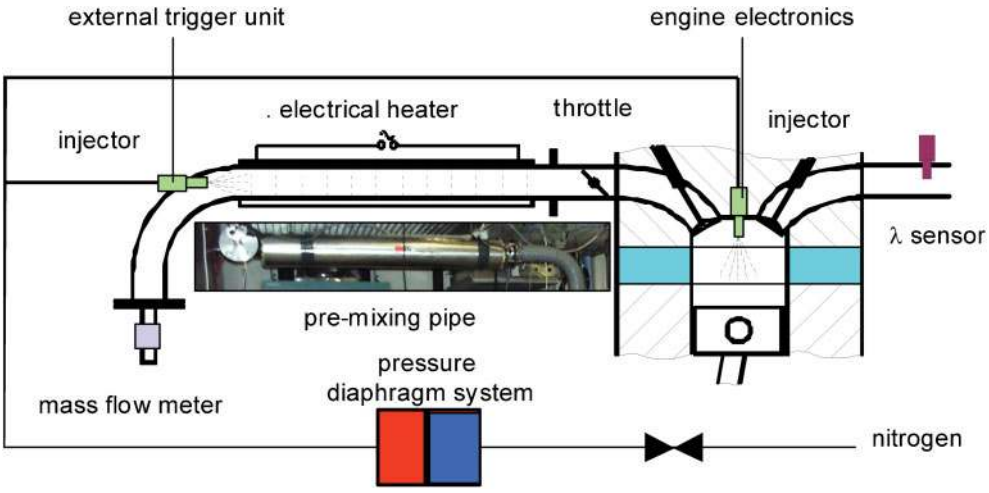

Fig. 3 Schematic of the premixing set-up

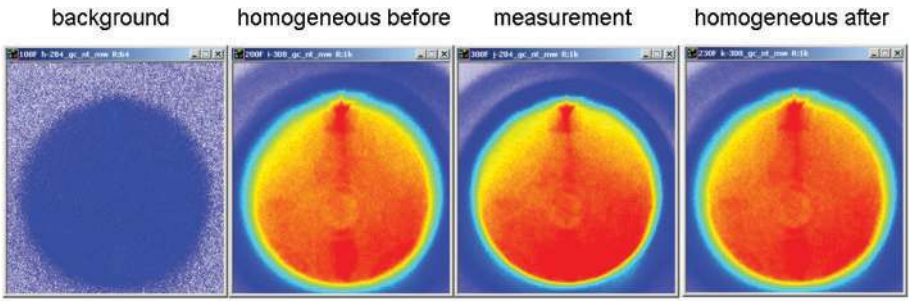

Fig. 4 Example images of one measurement procedure

3.2.2 *Evaluation of the optical measurements*

An averaged image with respective mean laser intensity was calculated from the 16 homogeneous images by evaluation software developed at the authors' institution. The averaged background image was subtracted from the mean homogeneous image – referring to the laser energy – to obtain the calibration image (at $\lambda = 1.0$), as well as from each direct injection image to obtain background corrected raw data. By comparing the averaged homogeneous images before and after direct injection measurements, a fouling coefficient can be calculated and included in the λ calculation. The intensity of the direct injection images is proportional to the calibration image. Thus, it was possible to calculate the λ-map of direct injection operation using the calibration images with a well known λ-value. Finally a 'contour' image marking important parts of the combustion chamber, such as the spark plug or the intake valves, was added on the 'result' image. All images presented are averaged from 16 single images at one crank angle position.

Parallel to each optical measurement, conventional engine datasets, including the pressure indication and temperature conditioning information, were also taken.

3.3 Two-line excitation LIF

For the two-line excitation technique, the two laser sheets with the different wavelengths of 248 and 308 nm were coupled to the engine through the piston window (see Fig. 5). A dichroic mirror was necessary for superposition, and a dual-wavelength mirror was installed in the elongated, slotted piston. An intensified double-shutter camera was used, and hence the two images were superposed automatically, and only one camera was necessary to take the images of both wavelengths. A 100 mm f/2.0 lens was applied, with suppression of the elastically scattered light by two serial 355 nm long-pass filters (attenuation 10^6 each). The temporal separation between the two laser pulses was set to 2 μs, and the image intensifier of the camera was gated with 240 ns for each image to avoid any possible phosphorescence from the acetone. The camera was equipped with a fast phosphor screen (P46) with a decay time of about 2 μs, to reach an intensity level lower than 1 per cent. Hence, no influence from the first image could be seen on the second image.

The excimer lasers (KrF for 248 nm and XeCl for 308 nm) can be driven with arbitrary frequencies, so the time synchronization of camera and lasers with the engine is straightforward.

To obtain the desired information, four images are necessary, two reference images with known physical state and mixture composition and two images at the desired crank angle position. This is typically noise enhancing. Therefore, beam homogenizers were used, which reduced the inhomogeneities in the spatial intensity profile of the light sheets to less than ± 5 per cent [**12**]. Additionally, the pulse energy for both wavelengths was recorded with energy scopes. Because of these supplementary components, the light sheets were coupled to the combustion bowl only through the piston window, which resulted in a smaller field of view. The field of view was defined by the diameter of this window, which is shown in Fig. 6. The light sheet plane is positioned 8 mm behind the spark plug centre and normal to the crankshaft. At the top, where the lasers hit the cylinder head wall, perturbing fluorescence could be observed, caused by oil and deposits. A special mask was therefore installed directly in front of the glass ring to suppress these signals.

In order to seed the tracer acetone into the intake air, a commercial direct injection valve was used instead of the fuel injector upstream of the mixing pipe. Here, pure acetone was added to the intake air.

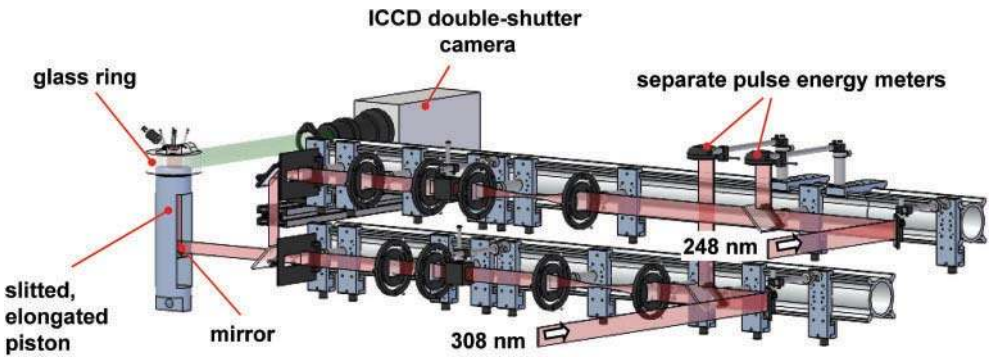

Fig. 5 Experimental set-up for the two-line excitation LIF technique

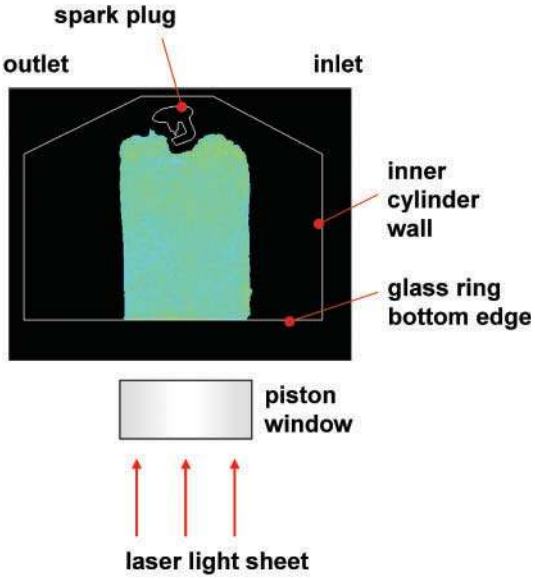

Fig. 6 Field of view for two-line excitation LIF

The amount was controlled by the injection frequency (one injection per working cycle) and opening time. Therefore, a free programmable magnetic valve drive was used. The acetone amount was calibrated in experiments before. For the acetone partial pressures used, heating of the mixing pipe was unnecessary, so the air could be sucked in with room temperature. The mixing of air and acetone was checked by the homogeneity of the motored images. During fired operation, the fuel was always directly injected into the cylinder.

3.3.1 In-cylinder measurement procedure

The engine measurements are structured in two main steps, the acquisition of the reference at known engine conditions and the acquisition of images at the different crank angle positions of interest.

The first step is the acquisition of images at the reference conditions in motored operation mode. In the present work, a reference point at 10° CA after electronic triggering of the injector (in motored operating mode without injection) of the high-pressure cycle was chosen. The pressure of the reference point was known from the conventional engine indication system. The gas composition was known as well, because in the motored operation mode only air and tracer are inside the cylinder. The temperature had to be estimated because of dynamic effects in the engine and because it was not possible to measure the temperature of the gas in the engine directly. To begin with, the estimation used was set at the mean value between the cooling water temperature of 353 K and the inlet air temperature of about 300 K at the position of the air mass flow sensor. Later, this temperature was corrected to 340 K with the aid of a polytropic fit. In addition to the images with tracer, images without the addition of tracer were acquired. These images were used as background, helping to remove last spurious signals.

In a second step, images at the crank angle position of interest were taken. Usually, 30 images for both wavelengths were collected at one crank angle position. For each crank angle position, three different operating conditions were measured. First, background images without tracer were taken, then images with acetone but without fuel, and finally images in fired operation mode. The amount of tracer was adjusted to the pressure, which changed with the crank angle position. For higher pressures near TDC, the acetone volume fraction was smaller than for measurements at lower pressures. One part of the amount of fuel was replaced with the tracer to achieve stoichiometric combustion. The volume fraction of acetone in the intake air was about 2 per cent. This large volume fraction was necessary because of the low pressures in the engine, down to less than 0.03 MPa. To achieve the same tracer density for 0.1 MPa manifold absolute pressures, the volume fraction could be reduced to less than 0.5 per cent. This is due to the increased fluorescence quantum yield for higher pressures. The pressure used for each crank angle position was calculated as a mean value of 50 cycles. It should be noted that the pressure can be considered as a global quantity in the combustion bowl (owing to the high speed of sound), whereas temperature and tracer density vary and must be used as locally resolved quantities. The images were computed in the form of temperature images and as images of the intake air fraction, i.e. complementary to the residual gas fraction.

For the image processing, the possible error caused by absorption of laser light by the tracer was evaluated. With the known absorption cross-section, the attenuation can be derived from the Beer–Lambert law. For example, for the calculation of temperature, a tracer density of about 0.05 kg/m^3 results in an error of less than 0.6 per cent because the absorption cross-section is of the same order of magnitude for both wavelengths. For the intake air fraction, the absorption error is less than 3 per cent.

4 RESULTS

All operating points shown have the same engine speed (1500 r/min) and indicated mean pressure

(0.2 MPa). The crank angle positions of the results shown are defined in degrees crank angle after electronic triggering of the injector (aETI). The characteristics of the investigated operating points are summarized in Table 2.

The investigated engine conditions vary in the in-cylinder flow situation as well as in the pressure difference between ambient (p_{amb}) and intake pressure (p_{in}). In the following, the results of the three operating points will be discussed separately. The first operating point (OP 1) represents the reference situation for the mixture formation of a DISI engine with one main component of the intake air streaming. The second operating point (OP 2) shows advantages concerning the load change and the overall efficiency due to the absence of a pressure difference between intake air and ambient conditions. Here a combination of swirl and tumble define the in-cylinder flowfield. However, a look at the engine indication data shows an increase in the cycle-to-cycle variations. In the last operating point (OP 3) the advantages in efficiency of OP 2 should be combined with the stability of OP 1. Therefore, the analysis of the flowfield of the first two operating points should be utilized for the definition of a new injection strategy.

4.1 Temperature and residual gas fraction results

A possible reason for the cycle-to-cycle variations is an inhomogeneous distribution of the residual gas at ignition time. The ignition limits can be changed by high concentrations of residual gas, and the ignitability of the fuel/air mixture is reduced in comparison with the same λ-value in pure air. The ignitability is interesting, especially near the spark plug where the combustion process starts. Therefore, the two-line excitation technique was applied to the two operating points OP 1 and OP 2 to measure the residual gas concentration. Of special interest are the processes of mixing of air and residual gas, as well as the quantification of the residual gas fraction. Residual gas nests cannot be identified in images of the fuel/air ratio because FARLIF images show a signal proportional to the ratio of fuel and oxygen. Hence, the signal strength is independent of the dilution of fuel/air mixtures by residual gas.

As a first examination, the distribution and fraction of residual gas was measured at ignition time. For quantification of the residual gas, a region of interest (ROI) was defined below the spark plug, and a spatial and ensemble-averaged value was determined for this region. The ROI is shown in Fig. 7 by the white frame for the actual measurement position. At both operating points, no inhomogeneities were observed. In the two-line excitation technique, the temperature is obtained as additional information because it is necessary for the evaluation of the intake air fraction. For OP 2 in Fig. 7, the temperature is shown in the left-hand image and the fraction of intake air on the right-hand side, which is the inversion of the residual gas fraction. Both images are single shots and show a relatively homogeneous distribution for the temperature as well as for the intake air fraction.

The measured values of temperature and residual gas fraction are given in Table 3 for the two operating points investigated. Whereas the temperature is nearly equal, the 22 per cent residual gas in OP 1 is 5 per cent greater than the amount of residual gas in OP 2. This could mean either that the total amount of residual gas in the cylinder is larger or that there are inhomogeneities outside the visible area.

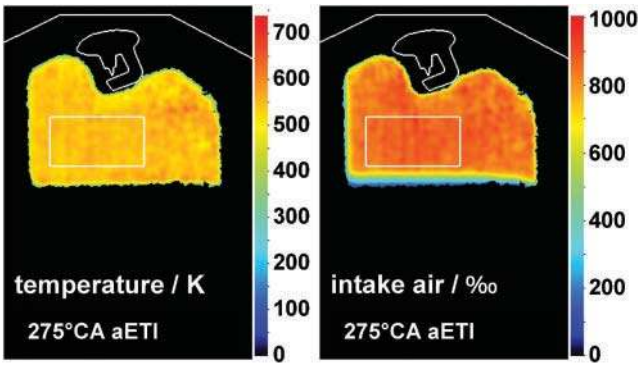

Fig. 7 ROI for temperature and residual gas fraction measurements to ignition time of OP 2. Single-shot images

Table 2 Operating points

Labelling	Mixture formation features
OP 1	Tumble, $p_{in} < p_{amb}$
OP 2	Swirl and tumble, $p_{in} \sim p_{amb}$
OP 3	Swirl and tumble, $p_{in} \sim p_{amb}$, double injection

Table 3 Temperature and fraction of intake air for different operating points at ignition time

	Temperature (K)	Fraction of intake air (%)
OP 1	544	22
OP 2	546	17

In addition to the measurements at ignition time, the temporal development of temperature and intake air fraction during the compression stroke is displayed in Fig. 8 for OP 2. At three selected crank angle positions, these data were also measured for OP 1. The temperatures of OP 1 show a nearly complete agreement with the OP 2 data. The fraction of residual gas is larger in OP 1.

The fluctuations in the residual gas fraction over the crank angle are partly a result of fluctuations in the measurement technique itself. The lower temperature at 270° CA aETI is due to a break in the measurements and the transient temperature increase after restart of the optical engine. More information about this transient behaviour can be found elsewhere [**7**].

In Fig. 9 the increase in temperature during the compression stroke is shown in an ensemble of single-shot images. In all images, a relatively homogeneous distribution of temperature and intake air fraction is visible. At 295° CA aETI, the flame front is visible directly beneath the spark plug. Here, the tracer acetone is consumed by the flame and so no signal can be observed behind the flame front. At 225° CA aETI, disturbances caused by oil are visible in the right-hand lower corner. Also, the connection between glass ring and cylinder head is visible as a pale horizontal line in the images. In the undisturbed areas of the image, the homogeneity is obvious, in particular closer to the ignition time at 275° CA aETI.

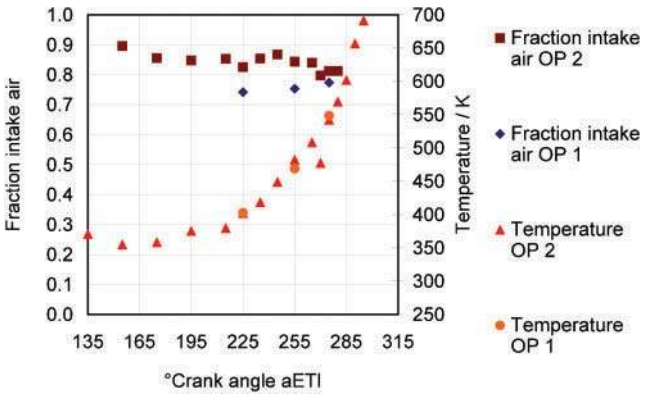

Fig. 8 Temperature during the compression stroke

Measurements during the intake stroke were performed to show the mixing of intake air and residual gas (see Fig. 10). Here, during the intake stroke, the gradients of intake air fraction disappear quickly. This fast mixing process results in a very homogeneous distribution of the residual gas at ignition time. The images are again time-resolved single shots. To avoid a perturbation by droplets, the injection was shifted by 45° CA after the actual electronic triggering of injection, i.e. the notation aETI was retained for the images, although the injection starts later. In regions with small intake air fractions, the signal-to-noise ratio of the tracer is too low and the evaluation software sets the values to zero. This can be observed at −5° CA and 5° CA aETI, where black regions are in the field of view. The inhomogeneities at 45° CA aETI result from disturbance of the oil film and do not represent the mixing process.

A closer look at the distribution of residual gas is given in Fig. 11 for both operation points at ignition time. Ensemble-averaged images are shown, and

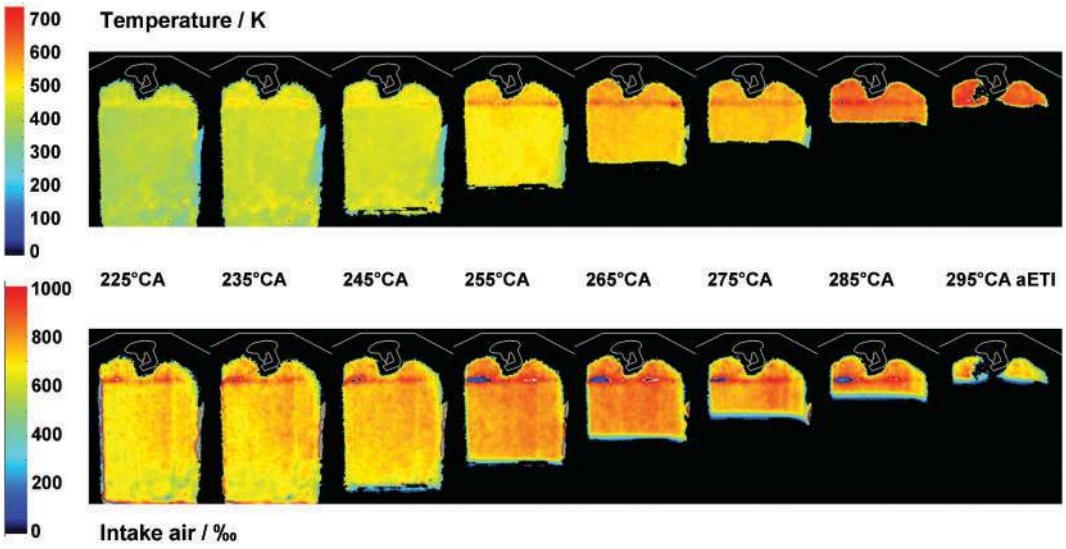

Fig. 9 Single shots during the compression stroke of OP 2

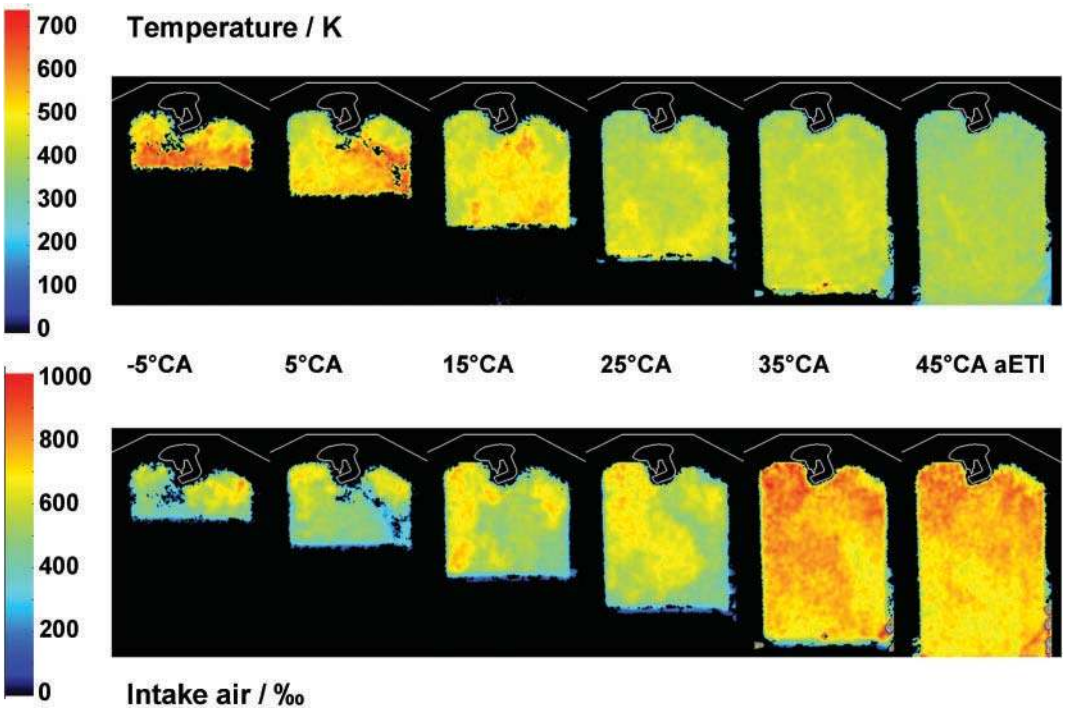

Fig. 10 Single shots of mixing of intake air and residual gas during the intake stroke

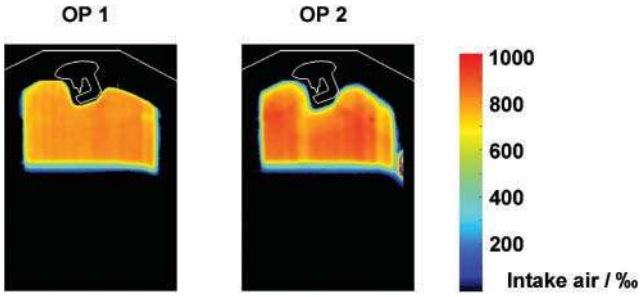

Fig. 11 Intake air distribution at ignition time. Ensemble-averaged images

very good homogeneity is visible. Only very small fluctuations are discernible in the field of view, which are partly caused by the measurement technique. In combination with the single-shot images, it is ascertained that no turbulent structures exist at any point in time, and nor do any global gradients exist in the mixture at ignition time. Hence, it can be assumed that effects of cycle-to-cycle variations are dominated by the preparation of the fuel/air distribution and not by inhomogeneities in the residual gas distribution.

4.2 Fuel/air ratio results

The presented results concerning the fuel/air mixture formation process form a combination of vertical and horizontal images according to Fig. 2. The false colour representation reflects the fuel/air mixing from the lower ignition limit (LIL) over stoichiometric conditions (stoich.) until the upper ignition limit (UIL). Owing to the different steps of the mixture formation process, a change and adaption of the scale will be used when necessary. The mixture formation will be analysed two dimensionally and quantitatively from the electronic start of injection until the ignition point.

4.2.1 Operating point 1 (OP 1)

During the injection of the liquid fuel, the signal intensities from the elastically scattered light are too high to allow a quantitative determination in the form of a λ-scale. Nevertheless, the propagation of the liquid phase and its interaction with the combustion chamber and the flowfield can be investigated. Figure 12 at 15° CA aETI shows one moment during that injection phase, displaying the fuel distribution in the VLLS and in the HLLS plane. Intake and exhaust regions as well as the position of the spark plug are indicated. This indication also holds for Figs 13 to 17. The liquid fuel hits the piston symmetrically at its centre and is reflected towards the exhaust area. The horizontal investigation plane shows the nearly unaffected spray pattern of the seven-hole high-pressure injection valve. On deflection from the piston, the fuel propagation exhibits the

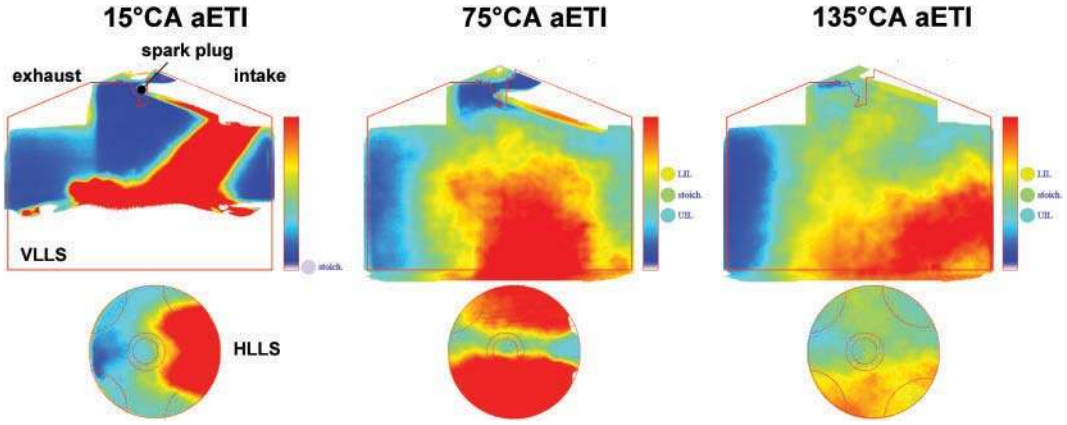

Fig. 12 Fuel/air ratio distribution for OP 1, intake stroke

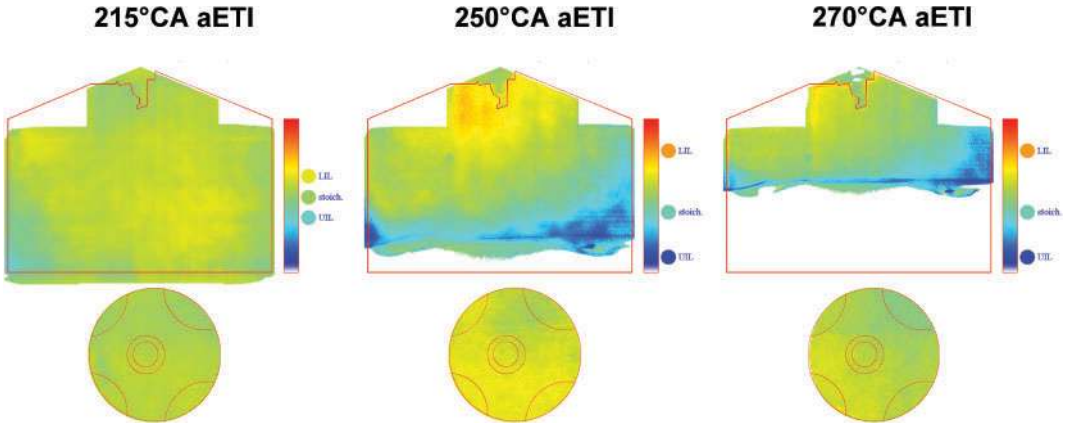

Fig. 13 Fuel/air ratio distribution for OP 1, compression stroke

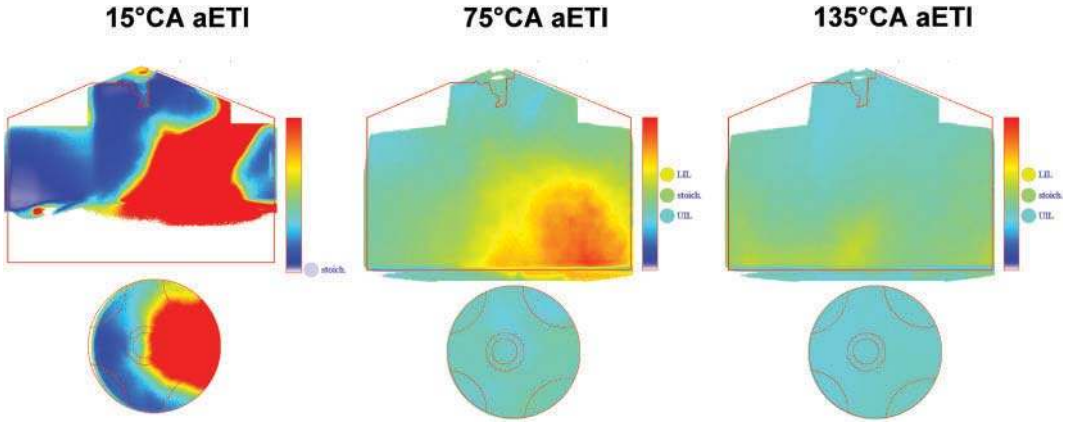

Fig. 14 Fuel/air ratio distribution for OP 2, intake stroke

actual injection momentum quite well. An interaction with the combustion chamber wall is suppressed by the opposite flow of the intake air tumble motion. Steady propagation of the single spray cones occurs during the complete intake phase.

The intake stroke phase is displayed in Fig. 12. At 75° CA aETI, the incipient mixture formation is presented. The formation of smaller droplets and their interaction with the tumble flow results in the state presented. The reduced momentum of the small fuel elements and the proceeding decomposition of the kinetic energy lead to a circulation of the fuel/air cloud into the middle of the combustion chamber. Owing to the absence of a swirl component of the

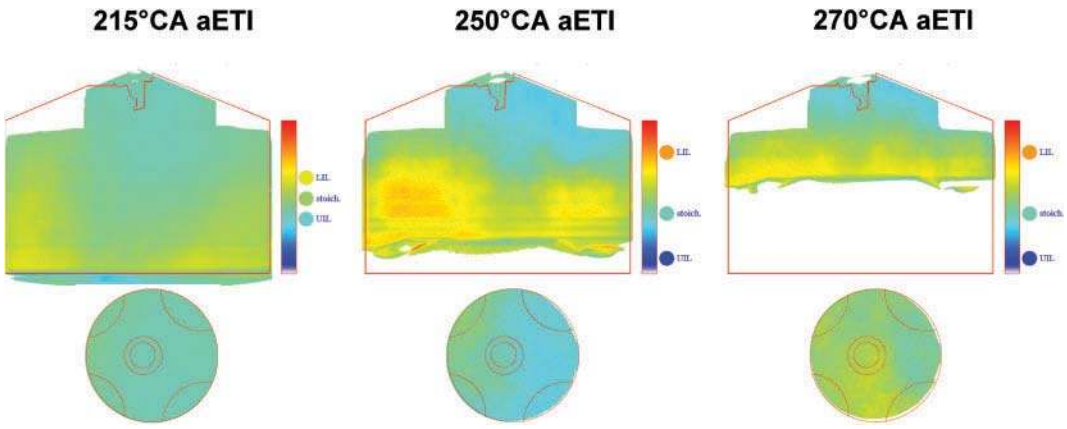

Fig. 15 Fuel/air ratio distribution for OP 2, compression stroke

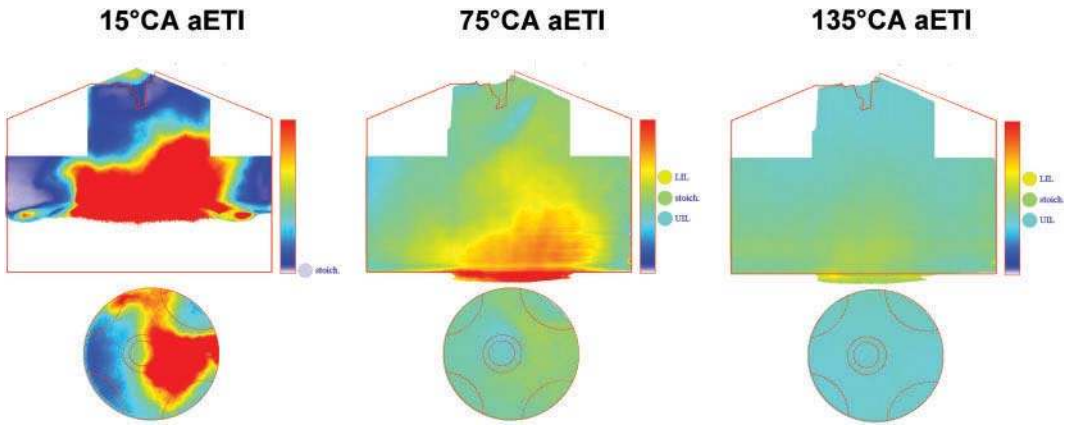

Fig. 16 Fuel/air ratio distribution for OP 3, intake stroke

intake air flow, the original subdivision of the distinct spray cones can still be seen, whereas the activity of the tumble motion becomes apparent in the turned structure of the charge cloud. The fuel-rich centre of this structure is located at the bottom of the investigation plane in the middle of the combustion chamber and becomes leaner towards the outer areas. During the ongoing intake stroke, the piston moves down until the bottom dead centre.

The two-dimensional distribution of the fuel/air ratio at this moment is displayed in Fig. 12 at 135° CA aETI. The fuel-rich centre of the charge cloud has been moved towards the intake area, and the bulk is still visible in the investigation plane and has not

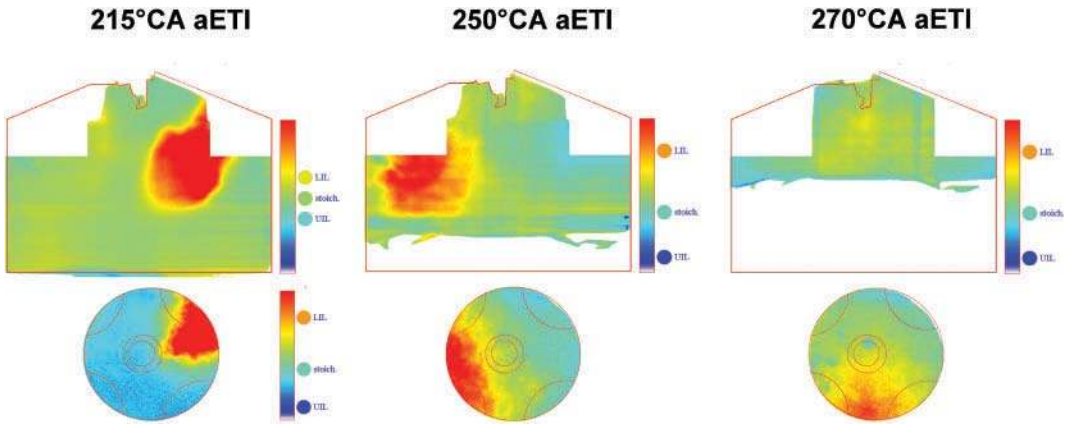

Fig. 17 Fuel/air ratio distribution for OP 3, compression stroke

been moved out of it by the piston motion and its suction effect. Thus, even at this early point in time, fuel-rich conditions exist in the area of the spark plug. Furthermore, a rotation of this structure and, with this, a mixing of the fuel and air can be observed. In the horizontal plane, a dislocation of the previous symmetrical development of this process becomes apparent, with areas richer in fuel towards the observer. Besides the charge motion, there are two more reasons for this. First, the piston window is not located in the centre of the piston bottom, to maintain functioning parts of the bowl. Second, the seven spray cones enter the combustion chamber asymmetrically.

Figure 13 displays the compression stroke phase of OP 1. The mixture distribution at an early point of compression is shown at 215° CA aETI. Along with the compression of the charge, further mixing of fuel and air occurs, leading to fuel-rich conditions throughout the combustion chamber. While the piston is moving upwards, this process is supported by the tumble motion. This can also be seen in the rotation of the charge cloud from the intake region into the spark plug area. Also, the tumble motion is destroyed during the compression phase, and this mixture flow is not conducted and induced by the piston action. Thus, no direct contact of the fuel cloud and the piston can be observed. Whereas in the range of the bottom dead centre a preference for mixture distribution in the horizontal plane towards the observer could be observed, a total change in this situation is now seen. The view through the piston shows a nearly perfect, homogeneously mixed, and fuel-rich charge.

In order to improve the analysis of the mixture situation and the degree of homogenization, the λ-scale is expanded in the next image at 250° CA aETI. With this zoom it is possible to have a larger range of values within the false colour representation. The situation shortly before ignition is shown in Fig. 13 at 270° CA aETI. The previously described processes and their outcome can clearly be seen in the fuel/air distribution at the ignition point. Although the tumble motion has been destroyed during compression, there is still no contact of the charge cloud with the piston. The result is a very good mixture situation for ignition. The area around the spark plug shows fuel-rich conditions, whereas it becomes leaner towards the borders. Thus, the desired conditions for DI operation are achieved, and a stable start of the combustion reaction can be ensured. Within the horizontal plane, the differences in relation to the previous crank angle position are negligible. This operating point reveals nearly ideal mixture formation conditions and thus forms the reference situation for the following comparison with OP 2.

4.2.2 Operating point 2 (OP 2)

Owing to the absence of a pressure difference between intake air and ambient conditions, this operating point shows advantages concerning the load change and the overall efficiency. However, a look at the engine indication data shows an increase in the cycle-to-cycle variations. The origin of this characteristic behaviour will be clarified by the mixture formation analysis. Here, the in-cylinder flowfield and in particular the swirl and tumble motion of the air are of special interest. Figure 14 shows the intake stroke phase of OP 2, and Fig. 15 shows the compression stroke phase of OP 2.

Figure 14 shows the interaction of intake air and injected fuel at 15° CA aETI. Similarly to OP 1, the fuel jet hits the piston bowl at its centre but, owing to the in-cylinder air motion, the redirection is much less developed. The activity of the swirl component becomes apparent through the compressed structure of the spray cones, which can be seen in the image of the vertical investigation plane. With continuing injection and air intake, the liquid fuel is centred on the piston in the middle of the combustion chamber. The radial flow component inhibits spray propagation towards the exhaust side almost completely. After the end of injection, and with increasing tumble motion, the fuel/air cloud is pushed out of the horizontal centre area into the activity region of the radial swirl motion. The superposition of the in-cylinder flow components and their great influence on the fuel/air mixing result in a locally concentrated charge following the streaming. The ongoing downstream movement of the piston and its suction effect support this process. Thus, the position of the fuel/air cloud is at the bottom of the vertical investigation plane, as can be seen in Fig. 14 at 75° CA aETI. At this point in time, the active area of the fuel/air mixing of OP 1 is due to the tumble motion being more widespread in the vertical plane. In contrast to this, the complex superposition of radial and axial flow at OP 2 shows a more concentrated mixture situation on the top of the piston. The increasing activity of the tumble motion can be seen in the bulging of the charge cloud on the intake side. However, the fuel/air ratio in the roof area of the combustion chamber is mostly lean and at the upper ignition level. With a continuing intake cycle, the previously described tendencies and trends become increasingly apparent.

The mixture situation around bottom dead centre is displayed in Fig. 14 at 135° CA aETI. The stratification effect of the charge is very obvious. Almost the complete injected fuel mass is located in the region of the piston, building a fuel-rich area that shows a very sharp boundary towards the very lean remaining parts of the combustion chamber. The horizontal plane below the spark plug shows nearly no fuel/air mixture at all. The low λ-ratios above the piston in combination with the ω-shaped structure of the charge cloud on the piston shows the dominating effect of the swirl motion at OP 2. The positive mixture formation effect of the tumble flow at OP 2 is superposed and suppressed by the radial streaming.

The further development of these processes during the first compression phase is displayed in Fig. 15. The previously described mixture stratification is still present during the upward stroke of the piston at 215° CA aETI, whereas the middle section of the combustion chamber shows mostly lean mixture conditions. The investigations of the horizontal laser light sheet underline this distribution. Owing to tumble but mostly swirl motion, the areas on the intake and exhaust side are mixed very well. Thus, in contrast to OP 1, the fuel/air mixture is moved upwards with the piston motion and is not circulated by the axial streaming. This leads to the undesired stratification situation with very lean regions in the area of the spark plug. With increasing in-cylinder pressure, the situation becomes worse as the tumble motion is destroyed and the radial swirl flow remains active. Thus, mixing in the vertical plane is almost totally disabled, and the charge is prepared only horizontally on the piston.

The resulting mixture distribution at the ignition point can also be seen in Fig. 15 at 270° CA aETI. The charge stratification of OP 2 leads at that point to the exact opposite to the desired fuel/air mixture at ignition. In contrast to OP 1, the region directly around the spark plug shows stoichiometric and lean conditions, while the fuel-rich areas are located on the piston. Thus, the ignitability of the charge is influenced by the cycle-to-cycle variations. The origin for this behaviour can be found in the dominant effect of the swirl flow during the compression stroke. As the tumble motion becomes weaker and is finally destroyed, the axial rearrangement towards the spark plug is also reduced and only the radial flow mixes the charge cloud. Thus, the in-cylinder streaming no longer supports the motion of fuel-rich regions towards the spark plug. With this kind of mixture preparation, a stable and reliable operation of the engine at varying ambient conditions seems to be difficult to accomplish. In order to preserve the positive effects of the gas exchange and residual gas distribution, and to generate a good fuel/air distribution at the ignition point for the start of the combustion reaction, a change in the operational mode has to be carried out. Different possibilities concerning the hardware and software, such as injector targeting and timing or rail pressure variations, were taken into account. Moreover, multiple injection strategies are a widely used technique in this context.

4.2.3 Operating point 3 (OP 3)

The use of a double-injection strategy has proved to be a very good and easy method for optimization of the engine process [**13**]. In the present investigation, splitting of the total injection mass into two parts was applied, one large part into the intake stroke and a smaller part into the compression stroke. As the amount and the timing of the second injection can be combined in several different ways, this strategy represents a significant increase in the complexity of the systems. The next operating point, OP 3, shows a good combination of these factors in addition to the existing injection characteristics of OP 2. As the reduction in the mass of the first injection is not tremendous, the differences in the mixture formation during the intake stroke in comparison with OP 2 are negligible. This can be seen in Fig. 16, where the intake stroke of OP 3 is displayed. The fuel/air distribution in Fig. 16 at 135° CA aETI shows the starting situation for OP 3 at the beginning of the compression stroke. As expected, the fuel/air distribution is nearly identical to OP 2 at bottom dead centre. Most parts of the mixture cloud have been sucked down with the piston. Therefore, the roof area of the combustion chamber shows very lean mixture conditions, and only in the lower region can stoichiometric values be found. As the compression continues and the in-cylinder pressure rises, the mixture distribution becomes nearly identical to that at OP 1. The charge cloud moves upwards with the piston motion and shows mainly stoichiometric conditions. The knowledge of the actual fuel/air distribution is of great importance for the classification and further analysis of the effectiveness and the potentials of this measure. Shortly before the second injection, the fuel/air mixture situation is as follows. It is a stratified distribution with stoichiometric fuel/air ratios in the lower regions of the visible part of the combustion chamber and a strong leaning effect

towards the top. The addition of the smaller amount of fuel in the second injection takes place in the lean roof area of the combustion chamber. This can be seen in Fig. 17, where the spray propagation of the second injection at 215° CA aETI is displayed.

It is obvious that the spray penetration depth and the higher local accumulation of fuel are due to the smaller injection mass. Investigation of the horizontal laser light sheet already shows, at this early point in time after injection, a significant influence of the swirl motion on the radial propagation of the second injection. As the amount of liquid fuel within the horizontal laser light sheet is much smaller, and the resting time shorter, in comparison with the first injection, an expanded λ-scale can favourably be used at this point in time and also at later times. Therefore, the false colour representation of both investigations is not identical in this case. However, the corresponding values for the fuel/air ratio represent the same mixture situation. The interaction between the second injection and the already prepared fuel/air mixture of the first injection can be seen in Fig. 17 at 250° CA aETI. In comparison with OP 2, the addition of an extra fuel mass in the compression stroke changes the mixture formation strongly. The propagation of the second injection takes place in the lean areas of the already prepared charge. Owing to the lower momentum of this fuel injection, the influence of the in-cylinder streaming is much stronger. This effect becomes apparent in the temporal evolution (215 and 250° CA aETI) of the fuel propagation in the horizontal plane. Within these 35° CA, the cloud of the second injection travels counterclockwise through this plane, while it is mixed in the axial direction with the already prepared parts of the first injection above the piston.

Furthermore, two other effects become obvious within this time period: first, the dominant role of the swirl motion, which moves large parts of the injected mass in nearly the same horizontal plane on a radial streamline; second, the still active tumble motion at this early point of compression, which takes along the end of the spray cones and circulates them axially along the spark plug area in the roof of the combustion chamber. With the chosen time interval between the fixed first and the second injection, a favourable fuel/air mixture could be achieved. Owing to this adjustment, according to the in-cylinder flowfield, the second smaller amount of fuel is kept in the roof area of the combustion chamber. While the stratified charge is moved upwards with ongoing compression, the centroid of the second injection is moved closer to the wall of the combustion chamber. This can be seen in the horizontal plane as the structure changes from triangular towards semicircular. In contrast to OP 2, interaction of the second injected fuel mass with the in-cylinder streaming results in fuel enrichment in the area around the spark plug. Thus, the problem of undesired stratification of the first injection at this location is no longer of any consequence. Even with the destruction of the tumble flow with increasing in-cylinder pressure, the charge cloud of the second injection is pushed into the roof zone. Moreover, the swirl motion turns the fuel-rich parts further around towards the observer in the middle section of the combustion chamber between exhaust and intake. The resulting fuel/air distribution at ignition is shown in Fig. 17 at 270° CA aETI.

The most important difference in comparison with OP 2 is the significantly richer fuel/air ratio near the spark plug. The local propagation and the actual λ-values are dependent on the mass and the timing of the second injection. If the injected mass is too large or the injection time is too late in the compression stroke, it will result in a leaner mixture and thus in fuel/air ratios that are at or below the lower ignition limit. An undersized injected mass or an injection time that is too early will cause a comparable situation with OP 2 and will result in mixtures that are too lean.

5 CONCLUSIONS

The two-dimensional distribution of the fuel/air ratio, as well as of the temperature and residual gas, has been quantified inside a modern gasoline direct injection engine by using two different fluorescence tracer concepts. These optical measurement techniques have been applied with different investigation planes consecutively in one optical engine. To investigate the influence of the in-cylinder flowfield on the mixture formation of a DISI engine, three different operation points have been analysed, one with only a tumble motion of the intake air (OP 1), one with tumble and swirl flow (OP 2), and one based on OP 2 but with a split injection strategy (OP 3). The three operating points show different behaviours concerning effectiveness, gas exchange, and cycle-to-cycle stability. The reason for the difference in the stability of the combustion processes of OP 1 and OP 2 was of particular interest. It was found that at both operating points the residual gas was mixed very rapidly with the intake air during the intake stroke. The residual gas was distributed very homogeneously during the compression stroke, particularly at ignition

time. Hence, it can be assumed that the cycle-to-cycle variations found are not caused by inhomogeneities in the residual gas distribution but are dominated by the fuel/air mixture preparation.

The operating point with a single tumble motion of the intake air has been set as the reference situation. The mixture formation and preparation of OP 1 take place in a near-optimum way. The tumble motion circulates the injected fuel in the axial direction, whereas it remains in the upper part of the combustion and does not get sucked down with the piston during the intake stroke. While the tumble is destroyed with increasing compression, the well-prepared charge cloud remains in the roof area, showing fuel-rich regions at the spark plug and a leaning towards the piston. Thus, an ideal condition for the start of the combustion reaction exists at ignition time. Mixture formation investigations of DI operation with a superposed in-cylinder flowfield (OP 2) – swirl and tumble motion – showed a preparation of the injected fuel leading to stoichiometric or leaner conditions at ignition. The main reason for this behaviour is the dominant role of the swirl motion during compression. As the tumble flow is destroyed with increasing pressure, the prepared mixture is moved in the axial direction with the piston. Thus, a stratification of the charge results, with rich areas on the piston and a leaning effect towards the roof region. To change this, and to achieve the good load change properties of OP 2, a double-injection strategy (OP 3) was carried out. The first injection time was kept constant in the intake stroke, and the second injection was placed in the compression stroke. With the small mass of the second injection and the late injection time, the favourable mixture preparation according to OP 1 could be achieved. Owing to the low momentum of the second injection, the mixture preparation took place in the roof area. The swirl motion distributed the fuel above the already prepared charge of the first injection. With increasing in-cylinder pressure, the smaller cloud of the second injection was moved towards the spark plug, forming the desired fuel/air distribution at ignition time. The area in the roof of the combustion chamber shows fuel-rich conditions becoming leaner towards the piston area. These investigations also indicated the importance of an appropriate adjustment of mass and timing of the second injection with the in-cylinder flowfield. Both parameters and their variations – a mass that is too large or too small in combination with an injection time that is too early or too late – lead to an insufficient mixture preparation and not to an improvement in the engine process concerning ignition stability.

ACKNOWLEDGEMENTS

The authors gratefully acknowledge the financial support of parts of this work by the German National Science Foundation (DFG), which also funds the Erlangen Graduate School in Advanced Optical Technologies (SAOT) within the framework of the German Excellence Initiative.

REFERENCES

1 **Zhao, F., Lai, M.-C.,** and **Harrington, D. L.** Automotive spark-ignited direct-injection gasoline engines. *Prog. Energy Combust. Sci.*, 1999, **25**(199), 437–562.

2 **Hentschel, W.** Optical diagnostics for combustion process development of direct-injection gasoline engines. *Proc. Combust. Inst.*, 2000, **28**, 1119–1135.

3 **Thurber, M. C., Kirby, B. J.,** and **Hanson, R. K.** Instantaneous imaging of temperature and mixture fraction with dual-wavelength acetone PLIF. *AIAA*, 1998, 98–0397.

4 **Reboux, J.** and **Puechberty, D.** A new approach of planar laser induced fluorescence applied to fuel/air ratio measurement in the compression stroke of an optical SI engine. SAE paper 941988, 1994.

5 **Braeuer, A., Beyrau, F.,** and **Leipertz, A.** Laser-induced fluorescence of ketones at elevated temperatures for pressures up to 20 bars by using a 248 nm excitation laser wavelength: experiments and model improvements. *Appl. Optics*, 2006, **45**(20), 4982–4989.

6 **Schulz, C.** and **Sick, V.** Tracer-LIF diagnostics: quantitative measurement of fuel concentration, temperature and fuel/air ratio in practical combustion systems. *Prog. Energy Combust. Sci.*, 2004, **31**, 75–121.

7 **Löffler, M., Kröckel, K., Koch, P., Beyrau, F., Leipertz, A., Grasreiner, S.,** and **Heinisch, A.** Simultaneous quantitative measurements of temperature and residual gas fields inside a fired SI-engine using acetone laser-induced fluorescence. SAE paper 2009-01-0656, 2009.

8 **Fröba, A. P., Rabenstein, F., Münch, K.-U.,** and **Leipertz, A.** Mixture of triethylamine (TEA) and benzene as a new seeding material for the quantitative two-dimensional laser-induced exciplex fluorescence imaging of vapor and liquid fuel inside SI engines. *Combust. Flame*, 1998, **112**, 199–209.

9 **Daily, J. W.** Laser induced fluorescence spectroscopy in flames. *Prog. Energy Combust. Sci.*, 1997, **23**, 133–199.

10 **Koban, W., Koch, J. D., Sick, V., Wermuth, N., Hanson, R. K.,** and **Schulz, C.** Predicting LIF signal strength for toluene and 3-pentanone under engine-related temperature and pressure conditions. *Proc. Combust. Inst.*, 2005, **30**, 1545–1553.
11 **Koban, W., Koch, J. D., Hanson, R. K.,** and **Schulz, C.** Oxygen quenching of toluene fluorescence at elevated temperatures. *Appl. Phys. B Lasers Opt.*, 2005, **80**, 777–784.
12 **Pfadler, S., Beyrau, F., Löffler, M.,** and **Leipertz, A.** Application of a beam homogenizer to planar laser diagnostics. *Opt. Express*, 2006, **14**(22), 10-171–10-180.
13 **Rimmer, J. E. T., Garner, C. P., Hargrave, G. K., Richardson, D., Wallace, S.,** and **Long, E. J.** The influence of single and multiple injection strategies on in-cylinder flow and combustion within a DISI engine. SAE paper 2009-01-0660, 2009.

APPENDIX

Notation

E	pulse energy
k	rate
p	pressure
p_{amb}	ambient pressure
p_{in}	intake pressure
S	signal strength of fluorescence
T	temperature
η	optical efficiency
λ	wavelength
λ-value	air ratio
ρ	density
σ	absorption cross-section
ϕ	fluorescence quantum yield
Φ	fuel/air ratio
χ_i	molar species fraction

Abbreviations

aETI	after electronic triggering of the injector
CCD	charge-coupled device
DISI	direct injection spark ignition
EGR	exhaust gas recirculation
FARLIF	fuel/air ratio LIF
HLLS	horizontal laser light sheet
IC	internal combustion
ICCD	intensified CCD
LIF	laser-induced fluorescence
LIL	lower ignition limit
OP	operating point
SOI	start of injection
stoich.	stoichiometric
TDC	top dead centre
TEA	triethylamine
UIL	upper ignition limit
VLLS	vertical laser light sheet